NUMERICAL MODEL FOR FLAP-GATE RESPONSE TO TSUNAMI AND ITS VERIFICATION BY HYDRAULIC EXPERIMENTS

Yuichiro Kimura[1], Hideyuki Niizato[1], Kyouichi Nakayasu[2],
Tomohiro Yasuda[3], Nobuhito Mori[3] and Hajime Mase[3]

A flap-gate breakwater is a new type structure for coastal disaster reduction against tsunamis and storm surges. The breakwater usually lies down on the seabed and rises up as a seawall with its buoyancy when tsunami or storm surge occurs. In our previous experimental studies, wave blocking capabilities of the flap-gate against tsunamis were confirmed, and the characteristics of the gate motion and wave pressure have been clarified changing wave condition. Present study develops a numerical model considering fluid-body interactions for the flap-gate and validation of the numerical model is conducted. The numerical model consists of combining the overset grid method and level set method for solving both flap-gate motions and free surface water motions accurately. It is shown that the developed numerical model gives accurate predictions of flap-gate motions against hydraulic model experiments.

Keywords: flap-gate; tsunami; numerical simulation; fluid-body interaction; overset grid method; level set method

INTRODUCTION

Movable breakwaters that close the entrances of ports and rivers when tsunamis and storm surges occur are meritorious for reduction of coastal disasters. A flap-gate breakwater (referred to flap-gate, hereafter), as shown Fig.1, has been developed by Shirai et al. (2006), which is similar to the MOSE barrier constructed in Venice shown in Fig.2 (Lewin et al. 1990). Both the breakwater and barrier usually lie down on a seabed and rise up with buoyancy. There are differences between the flap-gate and MOSE barrier in the rising up direction and in the supporting method. Details of flap-gate are described in the Chapter2.

It was confirmed in the past hydraulic model experiments (Kimura et al. 2009; 2009; 2010) that the flap-gate having a support system using tension rods is effective against tsunamis. Present study develops a numerical model dealing with fluid-body interactions of the flap-gate and validates the numerical model.

Numerical studies for flap-gate type structures have been done by Tomita et al. (2003) and Kiyomiya et al. (2006) where these numerical models treat the structure as a part of fluid and the motion of structure is not interacted with flow. The numerical model of ALE (Arbitrary Lagrangian-Eulerian), using a transformed coordinate, is able to treat the interaction of waves and structures rigidly; however, calculation load is heavy because of re-structuring the coordinate according to the movement of structures.

The present study adapts the overset grids method (Obata et al. 1993) that possesses advantages of both accuracy and low calculation load. The overset grids method is a sort of finite difference methods, and numerical analyses are carried out by arranging finer grids (representing both flap-gate and transformed grids around the gate) on the coarser fixed grids. Modeling of gas-liquid interface is conducted by a level set method (Wada et al. 2005) that captures the interface using a distance function (a level set function *f*) which sets plus to the side of liquid phase and minus to the side of gas phase.

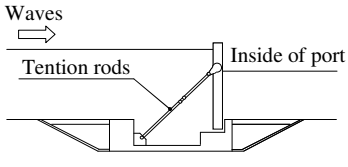

Figure 1. Proposed flap-gate breakwater

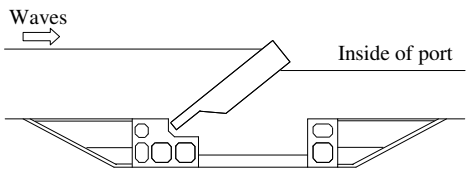

Figure 2. MOSE barrier

[1] Technical Research Institute, Hitachizosen Corporation, 2-2-11, Funamachi, Taisho-ku, Osaka 551-0022, Japan.
[2] Business Innovation Department, Hitachizosen Corporation, 1-7-89, Nanko-Kita, Suminoe-ku, Osaka 559-8559, Japan.
[3] Disaster Prevention Research Institute, Kyoto University, Gokasho, Uji, Kyoto 611-0011, Japan.

Flap-gate Breakwater

Figure 3 shows a sketch of the flap-gate motion when tsunamis and/or surges occur. The flap-gate, usually lying down on seabed, rises up through a sea surface with buoyancy, and then closes the entrance of port. The flap-gate stands up to the prescribed angle (90 degree in the figure (c)) by water level rise outside of the port. Tension rods, consisted of upper rods and lower rods, support forces of the flap-gate from water pressure. Resistance plates, as shown in Fig.3 (c), are installed between the lower tension rods. These resistance plates reduce the moving speed of rising up of the flap-gate. A substructure, shown in Fig.3 (a), holds the gate and tension rods and supports all forces by its weight.

The flap-gates are installed across a mouth of breakwaters like Fig.3 (e). The gap between each flap-gate is 1 % of its width. Since a prototype flap-gate is designed as 10 m width, the prototype gate gap is 10 cm. Because the tops of the flap-gates are bound together using wire ropes, each gate cannot move independently. Therefore, the gate interval does not increase. Each gate consists of vertical beams, horizontal beams, a shaft and a skin plate as Fig.3 (e). A couple of air tank have been installed between the vertical beams. The gate is designed as the gate can rise up by buoyancy of the one tank and traction of wire ropes from adjacent gates when the other tank has leaked. The end of tension rods is connected to the upper horizontal beam, and the other end of tension rods is connected to the substructure.

Since the lying gate has buoyancy by compressing air in tanks in normal circumstance, mooring wires keep the gate. Due to this system rising up time becomes shortened when a tsunami occurs. Buoyancy of the gate can be checked by measuring forces of the mooring system.

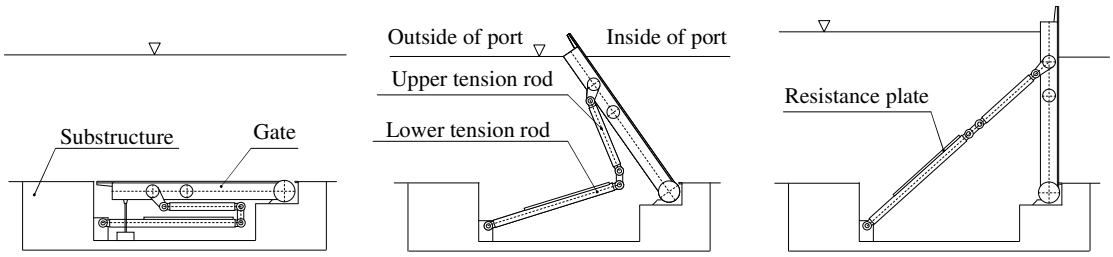

(a) Lying down on a seabed **(b) Rising up through a sea surface** **(c) Standing due to outside water level**

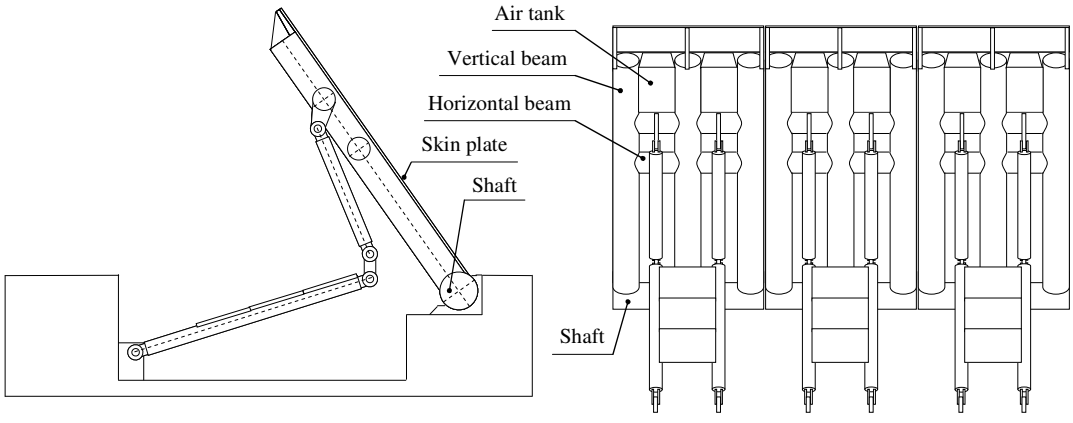

(d) Side view **(e) Flont view**

Figure 3. Behavior of flap-gate and side and front view of flap-gate

Governing Equations and Numerical Simulation Method

Governing equations. The governing equations are pseudo incompressible Navier-Stokes equations including pseudo time differentiation terms and are adopted in order to apply a pseudo compressibility formulation (Tanno et al. 2004). The continuity equation and momentum balance equations are described as

$$\frac{\partial p}{\partial \tau}+\frac{\partial u}{\partial x}+\frac{\partial v}{\partial y}=0\,, \tag{1}$$

$$\frac{\partial u}{\partial \tau}+\frac{\partial u}{\partial t}+u\frac{\partial u}{\partial x}+v\frac{\partial u}{\partial y}+\frac{\partial p}{\partial x}=\frac{1}{Re}\left[\frac{\partial^2 u}{\partial x^2}+\frac{\partial^2 u}{\partial y^2}\right]+f_x\,, \tag{2}$$

$$\frac{\partial v}{\partial \tau}+\frac{\partial v}{\partial t}+u\frac{\partial v}{\partial x}+v\frac{\partial v}{\partial y}+\frac{\partial p}{\partial y}=\frac{1}{Re}\left[\frac{\partial^2 v}{\partial x^2}+\frac{\partial^2 v}{\partial y^2}\right]+f_y \tag{3}$$

where p is the pressure, u and v are the velocities in the x and y directions, respectively, t is the physical time, τ is the pseudo time, Re is the Reynolds number, and f_x and f_y are the forces in the x and y directions, respectively.

The above equations become equivalent to incompressible Navier-Stokes equations when pseudo terms are neglected. Equations (1) ~ (3) are represented by using vectors as conservation system as

$$\frac{\partial \boldsymbol{q}}{\partial \tau}+\frac{\partial \boldsymbol{h}}{\partial t}+\frac{\partial \boldsymbol{E}_x}{\partial x}+\frac{\partial \boldsymbol{E}_y}{\partial y}+\frac{\partial p}{\partial x}=\frac{1}{Re}\left[\frac{\partial \boldsymbol{E}_{xu}}{\partial x}+\frac{\partial \boldsymbol{E}_{yv}}{\partial y}\right]+\boldsymbol{F}\,, \tag{4}$$

$$\boldsymbol{q}=\begin{pmatrix} p \\ u \\ v \end{pmatrix},\ \boldsymbol{h}=\begin{pmatrix} 0 \\ u \\ v \end{pmatrix}, \tag{5}$$

$$\boldsymbol{E}_x=\begin{pmatrix} u \\ u^2+p \\ uv \end{pmatrix},\ \boldsymbol{E}_y=\begin{pmatrix} v \\ uv \\ v^2+p \end{pmatrix}, \tag{6}$$

$$\boldsymbol{E}_{xu}=\begin{pmatrix} 0 \\ \partial u/\partial x \\ \partial v/\partial x \end{pmatrix},\ \boldsymbol{E}_{yv}=\begin{pmatrix} 0 \\ \partial u/\partial y \\ \partial v/\partial y \end{pmatrix}, \tag{7}$$

$$\boldsymbol{F}=\begin{pmatrix} 0 \\ f_x \\ f_y \end{pmatrix}. \tag{8}$$

A set of equations are solved by a finite difference method. Let the time step for the physical time Δt and an interval of the time step for the pseudo time $\Delta\tau$, the condition $\Delta t \geq \Delta\tau$ should be satisfied. The pseudo time means a time scale of internal repetition time to satisfy the compressibility of fluid.

Discretization of spatial differentiation. The inertial terms are discretized by a second order upwind differential scheme. For example, $\partial \boldsymbol{E}_x/\partial x_{(i,j)}$ is represented as

$$\left.\frac{\partial \boldsymbol{E}_x}{\partial x}\right|_{(i,j)}=\frac{E_{x(i+1/2,j)}-E_{x(i-1/2,j)}}{\Delta x} \tag{9}$$

where (i, j) is the grid numbers for the x and y directions, respectively. The diffusion terms are discretized by a third order central difference scheme. For example, $\partial \boldsymbol{E}_{xu}/\partial x_{(i,j)}$ is described as

$$\frac{\partial \boldsymbol{E}_{xu}}{\partial x_{(i,j)}} = \frac{2\boldsymbol{E}_{xu(i+1,j)}}{h_1(h_1+h_2)} - \frac{2\boldsymbol{E}_{xu(i,j)}}{h_1 h_2} + \frac{2\boldsymbol{E}_{xu(i-1,j)}}{h_2(h_1+h_2)} \tag{10}$$

where h_1 and h_2 are

$$h_1 = x_{(i,j)} - x_{(i-1,j)},\ h_2 = x_{(i+1,j)} - x_{(i,j)}, \tag{11}$$

respectively.

Time integration. The time derivative terms are described using a second order backward difference scheme as

$$\left(\frac{\partial \boldsymbol{h}}{\partial t}\right)^{n+1,m+1} = \frac{3\boldsymbol{h}^{n+1,m+1} - 4\boldsymbol{h}^{n} + \boldsymbol{h}^{n-1}}{2\Delta t} \tag{12}$$

where n is the step number for the physical time, and m is the step number for the pseudo time, respectively.

In this pseudo compressibility method, convergent solutions at each time step are necessary to get accurate solutions. The pseudo time integration is conducted by the LU-SGS method and rapid convergence of the solution at each time step was verified..

Overset Grid Method

Spatial interpolation of physical quantities. The overset grid method was originally developed to describe smoothly changing body surface with complex multi-body geometry (Matsuno et al. 1998). First the overset grid method uses the main grid which covers the entire flow field including the body. Second, subgrid mesh is overlaid on the main grid as shown in Fig.4. In the main grid system, the grid points inside of the body are excluded from the computation and are regarded as non-solution points ■ (called HOLE points, hereafter). The outside points of the body in the subgrid denoted by ○, are interpolated from the main grids at the first step of each pseudo time step. After obtained convergence solutions at each pseudo time step, the subgrid values are interpolated into the main grid points denoted as □ around the HOLE points. The flow field is solved on the main grid and on the subgrid simultaneously. Therefore, the both smaller and larger scale flow fields induced by the body are simulated by the subgrid and main grid scales, respectively and are fully computed together by the over grid method.

The HOLE points are boundaries outliner along the body surface. It is important to distinguish the grid points either inside or outside of the body. The HOLE points P on the main grid are classified by the following procedure. Firstly a point Q on the subgrid which is the nearest to the point P is selected. Secondly an inner product between an outward normal vector $\boldsymbol{n}$ from the point Q and a location vector $\boldsymbol{a}$ to the point P is calculated. If the inner product between the two vectors is positive, then the point P is not included in the HOLE boundary. On the other hand, and the point P is included in the boundary in the case that the inner product is negative as follows:

$$(\boldsymbol{n},\boldsymbol{a}) = \begin{cases} \le 0 & \text{HOLE} \\ > 0 & \text{Not HOLE} \end{cases}. \tag{13}$$

It is decided whether the main grid points are interpolated from every subgrid points with inequalities:

$$\begin{aligned} f_{AB}(x_P, y_P) f_{AB}(x_G, y_G) f_{CD}(x_P, y_P) f_{CD}(x_G, y_G) \ge 0 \\ f_{BC}(x_P, y_P) f_{BC}(x_G, y_G) f_{DA}(x_P, y_P) f_{DA}(x_G, y_G) \ge 0 \end{aligned}. \tag{14}$$

Here index A, B, C and D are apexes of a cell including the point P (see Fig.4), $f_{AB}(x, y) = 0$ is the straight line AB, (x_P, y_P) is the coordinate of the point P, and (x_G, y_G) is the arbitrary point in the cell ABCD, respectively.

The two dimensional linear interpolation is used from subgrid to main grid system:

$$\begin{bmatrix} x_P \\ y_P \\ q_P \end{bmatrix} = (1-X)(1-Y)\begin{bmatrix} x_A \\ y_A \\ q_A \end{bmatrix} + X(1-Y)\begin{bmatrix} x_B \\ y_B \\ q_B \end{bmatrix} + XY\begin{bmatrix} x_C \\ y_C \\ q_C \end{bmatrix} + (1-X)Y\begin{bmatrix} x_D \\ y_D \\ q_D \end{bmatrix}. \tag{15}$$

The location X and Y are solved from the first two equations in Eq.(15), and using computed X and Y the physical quantities q_p are obtained sequentially. Similarly, the physical quantities of the main grids are interpolated into the outliner of body in the subgrid by the same procedure.

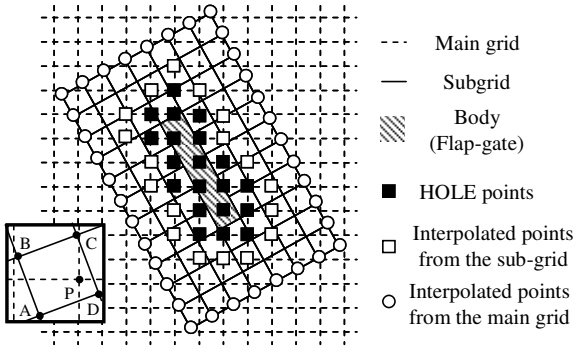

Figure 4. Ovelaying the body-fitted subgrid on the main grid

Moving body. A displacement of flap-gate motion is solved from the equations of motions integrating fluid forces acting on the body and an inertial moment of the body. The momentum acting on the body is obtained by integrating the pressure and the viscous forces multiplied by the distance from the rotational center over a circuit of the body. To obtain the ideal motion of the body and numerical stability, the iteration-adaptive grid generation procedure is repeated and iterated until a convergence of compressibility of fluid is satisfied.

Level Set Method

Capturing interface. A scalar function f so-called a level set function is introduced into the formulation of multiphase flow (Yang et al. 2005). The level set method can capture the accurate interface between two fluids without diffusion of grid scale. The level set function f is defined over the whole of computational domain and the function f is chosen as the signed algebraic distance to the interface, being positive in the liquid phase and negative in the gas phase.

The level set function also prescribes a finite thickness α of the interface and distributes the values such as density and coefficient of viscosity, changing sharply on the interface, among the thickness of the interface. Therefore numerical instabilities capturing at the interface can be avoided. Density and coefficient of viscosity using the level set function f are defined as:

$$\rho = \begin{cases} \rho_w & f \geq \alpha \\ \rho_a & f \leq -\alpha \\ \tilde{\rho} + \Delta\rho/2 \cdot \sin\left(\pi f/2\alpha\right) & otherwise \end{cases}, \qquad (16)$$

$$\mu = \begin{cases} \mu_w & f \geq \alpha \\ \mu_a & f \leq -\alpha \\ \tilde{\mu} + \Delta\mu/2 \cdot \sin\left(\pi f/2\alpha\right) & otherwise \end{cases} \qquad (17)$$

where ρ_w and ρ_a are the densities for liquid and gas, μ_w and μ_a are the coefficients of viscosity for liquid and gas, the tildes over the density and viscosity denote the averages of densities or coefficients of viscosity, and Δ denotes the difference between both of them, respectively. Figure 5 shows the schematic view of interface and level set function f according to the level set method.

The values of the level set function f are calculated from the following advection equation:

$$\frac{\partial f}{\partial t}+\left(\mathbf{u}\cdot\nabla\right)f=0\,, \tag{18}$$

where $\boldsymbol{u}$ is the velocity computed by Eq.(2) and (3).

Re-initialization of level set function. After some iteration steps, the function f will no longer remain a distance function (i.e., $\left|\nabla f\right|\neq 1$), generally, even if Eq. (18) advances the interface at correct velocities. Maintaining f as a distance function is very essential for accurate interface capturing. Therefore, a re-initialization procedure for recovering f as an exact distance function should be adopted to keep the interface thickness within finite value and preserve mass conservation. The re-initialization is done by equations as:

$$\frac{\partial f}{\partial \tau}=sgn\left(f^0\right)\left(1-\left|\nabla f\right|\right), \tag{19}$$

$$sgn\left(f^0\right)=\frac{f^0}{\sqrt{\left(f^0\right)^2+\varepsilon^2}} \tag{20}$$

where f^0 is the level set function at any physical time, i.e., $f^0(\boldsymbol{x}) = f(\boldsymbol{x}, \tau = 0)$, τ is the pseudo time in a re-initialization step, ε is the small value, and $sgn(f)$ denotes the smoothed sign function with appropriate numerical diffusion to avoid any numerical difficulties.

Equations (19) and (20) denote modification of a gradient of the level set function $\left|\nabla f\right|$, and thus the modified level set function f is employed as an initial value for the next physical time step. The distance function is reset without searching for an accurate location of the interface.

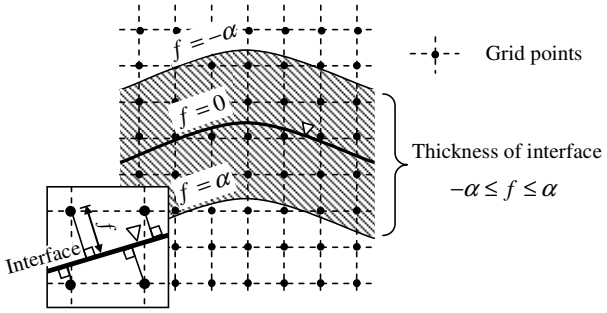

Figure 5. Interface according to level set method

Hydraulic Model Experiments

Solitary wave experiments. A series of experiments was carried out by using a 1/30 scale physical model in a two-dimensional glass-walled wave flume with 50 m in length, 1.0 m in width, and 1.5 m in depth located at Disaster Prevention Research Institute, Kyoto University. Figure 6 shows a sketch of experimental setup for the solitary wave experiments. A prototype structure is expected to build on a sea of 13 m depth, currently. The prototype structure is designed 22 m high and the corresponding experimental model gate is 71.7 cm high. In the wave channel, the bottom bathymetry consists of 1/10 slope along 4 m at the leading edge and is connected to 1/100 slope along 10 m, as shown Fig.6. The bottom bathymetry was built with sand and a semi-permeability mat on the sand surface. The flap-gate physical model was installed behind the slope and the foundation was built with aggregate. The water depth at the flap-gate was 42.4 cm.

Eight wave gages denote H11 ~ H18 were installed to measure a time series of water surface elevating. The gage H11 was set at offshore side of the 1/10 slope, H12 was set at a starting point of the 1/10 slope, H13 was set at a border between the 1/10 slope and the 1/100 slope, H14 and H15 were located over the 1/100 slope divided equally into three, H16 was set just front of the flap-gate model, H17 was set just behind the flap-gate model and H18 was set at 4 m behind H17, respectively. The flap-

gate motion angle was measured using an acceleration meter installed on the rotation center of the flap-gate. Photo.1 shows the experimental flap-gate model.

A solitary wave was generated by a computer controlled piston-type wave generator. Wave height of solitary wave at H11 was 12 cm, and wave height and wave period for prototype corresponded to 3.6 m and 166 s, respectively.

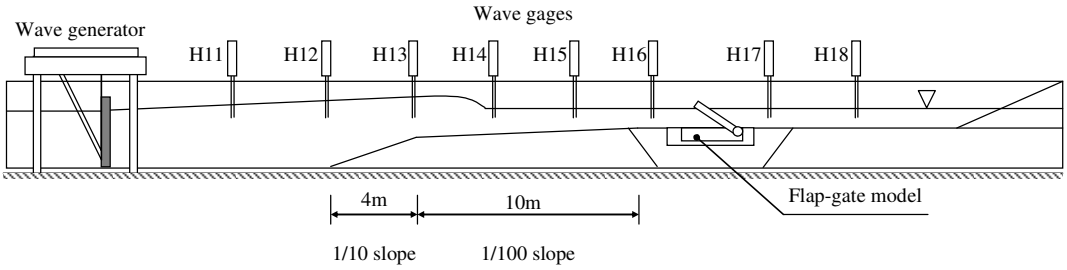

Figure 6. Experimental setup of solitary wave experiments

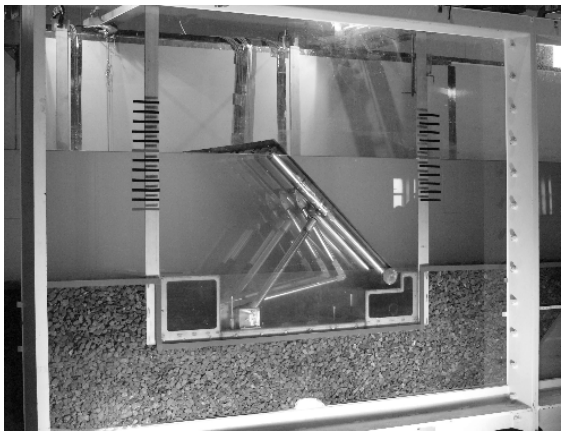

Photo 1. Flap-gate model in solitary wave experimental flume

Periodic wave experiment. The experiments for periodic wave experiments were conducted in a two-dimensional wave channel with 50 m in length, 1.0 m in width, and 1.2 m in depth located at Hitachizosen Technical Institute. The same flap-gate model with the solitary experiments was employed. Figure 7 shows a sketch of the experimental facility.

Two offshore wave gages (H21 and H22) and two onshore wave gages (H23 and H24) were installed to divide incident and reflective waves in both side of the flap-gate. The flap-gate angle was measured by the same instrument to the solitary wave experiments. Incident waves with wave period of 1.44 s, 1.81 s and 2.17 s were employed and wave steepness was fixed on 0.02 or 0.04. Table 1 shows the experimental wave condition.

Table 1. Wave condition in waves experiment

Prototype scale	Experimental model scale		
Wave period [s]	Wave period [s]	Wave height [cm]	
		H/L = 0.02	H/L = 0.04
8.0	1.44	5.08	10.2
10.0	1.81	6.71	13.4
12.0	2.17	8.28	16.6

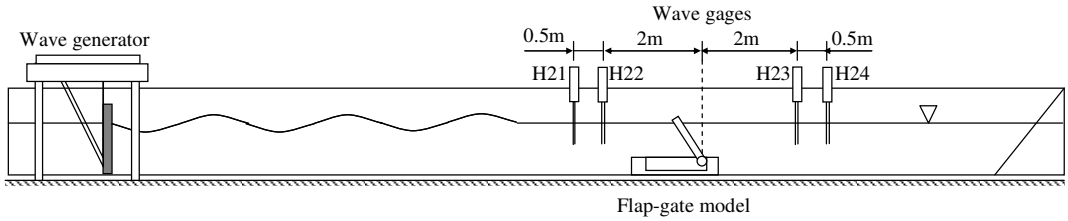

Figure 7. Experimental setup of periodic wave experiments

Numerical Results

A series of numerical simulation for flap-gate was conducted in a numerical wave channel with 27.6 m in length, as shown in Fig.8. The water depth was set as same as the hydraulic experiments. Number of the grid in the main domain was consisted of 440 grids in a horizontal direction and 65 grids in a vertical direction, respectively. The minimum main grid size was 20 mm in the main grid system. The subgrid domain was consisted of 75 grids in the gate height direction and 30 grids in the gate thickness direction, and the flap-gate consisted of 60 × 5 grids. The minimum grid size was 12 mm in the subgrid system. In hydraulic experiments, the flap-gate motion angle does not exceed 90 degree by supports of tension rods. The numerical flap-gate model was, therefore, forced do not to exceed 90 degrees. In these simulations, the resistance plates were not taken into account because it is three dimensional component of the system. Experimental cases without resistance plates were employed when comparing the simulations with the experimental results.

The offshore and onshore boundaries were set as wave incident boundary and wave radiation boundary, respectively. As the incident condition, long and small amplitude wave was used for the solitary wave and the Stokes wave with finite amplitude was used for the periodic waves.

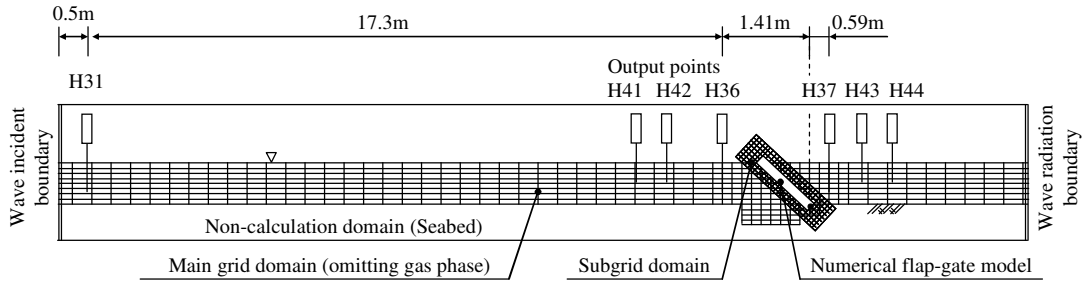

Figure 8. Illustration of Nnumerical domain

Comparison between Experimental and Numerical Results

Solitary wave experiment. Figures 9 and 10 show time series of water surface elevations and the flap-gate motions for the solitary waves both the hydraulic model experiment and the numerical simulation, respectively. The time series of experimental water surface elevations in Fig.9 (a) were measured at H11, H16 and H17 in Fig 6, and the time series of numerical one in Fig.9 (b) are at H31, H36 and H37 in Fig.8.

As shown in Fig.9, there is difference between the numerical water surface elevation at H31 and experimental one at H11. Since the offshore water depths in the experiments and the simulations are different, each the solitary wave velocities are also slightly different. In comparison of numerical solitary wave velocities and theoretical long wave velocities in very shallow water ($h/L \leq 1/25$, h: water depth, L: wavelength), both of them give quite reasonable accuracy. The water elevation by the numerical result at H36 shows a little different from the experimental result at H16. However, the water

elevation which was rising by reflection of the flap-gate and the variations of the wavy surface almost the same as the experimental result at H16. As concerns numerical result at H37, blocking a solitary wave and the variations of surface are similar to the experimental result. However, the experimental result of onshore water surface elevation is higher than the numerical one after flap-gate has risen up because it is due to water leak from outside of the flap-gate which has raised the inner water elevation in the hydraulic experiment. In the numerical simulation, such a water leak does not occur. Thus, the onshore side water surface elevation of numerical results is higher than experimental results. As shown in Fig.10, the time series of the flap-gate angle of numerical result quite agree with the experimental result.

Figure 11 shows snapshots of the flow vectors by the numerical simulation before and after the flap-gate raised up. Figures 11 (a) ~ (f) are velocity field at 0.32 s intervals. The white lines are computational grids, the domain composed by the vectors is the liquid phase and the lower domain colored by grey is the seabed or the substructure. The lines along the numerical flap-gate consist of the subgrid. The flow field on the subgrid is solved closely and subgrid rotates together with the flap-gate motion.

As shown in Fig.11 (a) ~ (d), the flap-gate gradually rises according to the wave forces acting on it. Since the flap-gate presses the onshore side water, the flow is advected to inside of the flap-gate. Figure 11 (d) shows the flow vectors at the time that the flap-gate just has stood up. Because the gate angle is limited up to 90 degrees and the flap-gate stops suddenly, the vectors in front of the flap-gate turn offshore and the surface variations are propagated offshore in wavy shape. Therefore, the wavy surface variations at H16 or H36 which are shown in Fig.9 (a) or (b) can be occurred due to the flap-gate movement close to 90 degree angle.

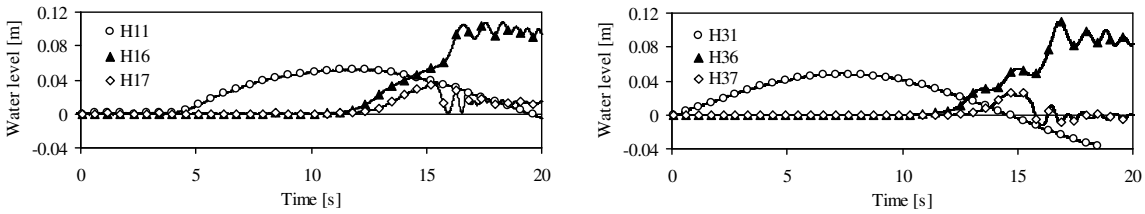

(a) Experiment **(b) Simulation**

Figure 9. Time series of water surface elevations

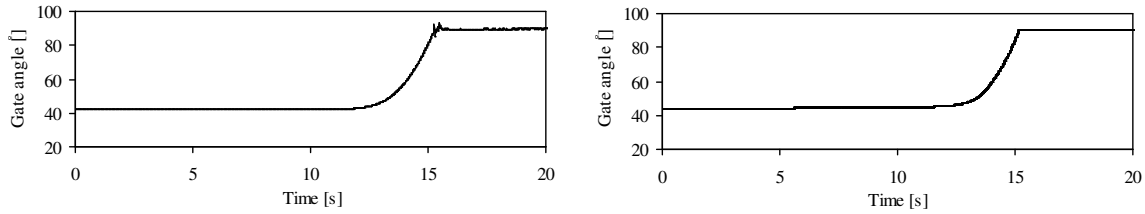

(a) Experiment **(b) Simulation**

Figure 10. Time series of flap-gate motions

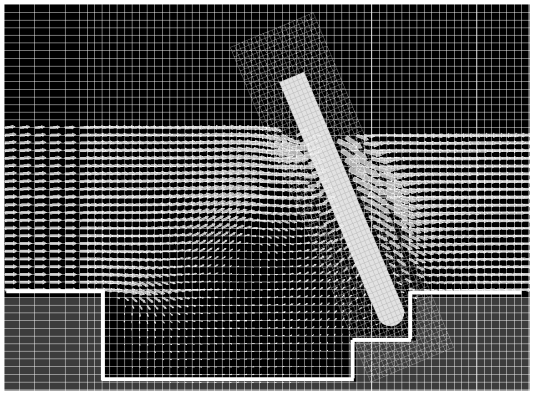

(a) Gate angle: 68 deg.

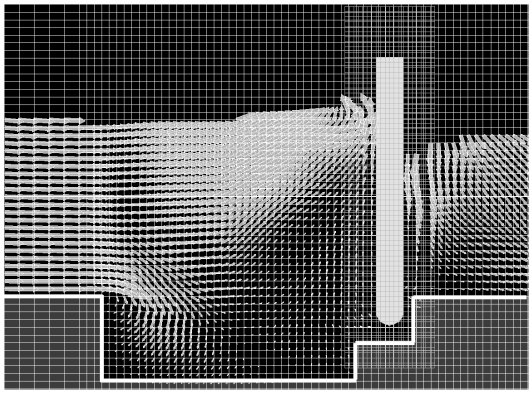

(d) Just standing up at 90 deg.

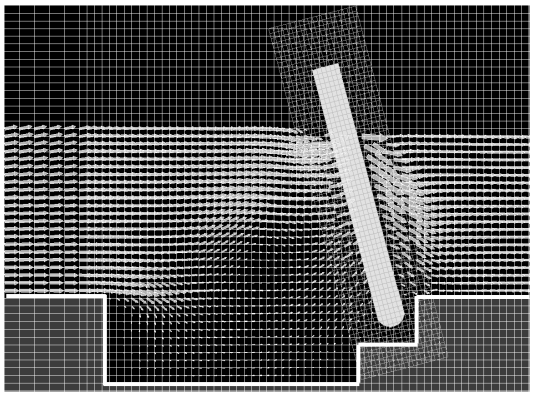

(b) Gate angle: 76 deg.

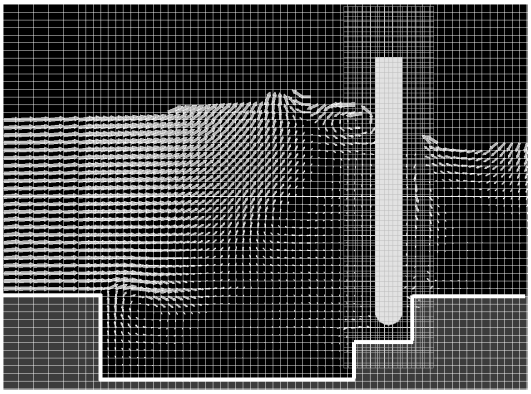

(e) 0.32 s after standing up

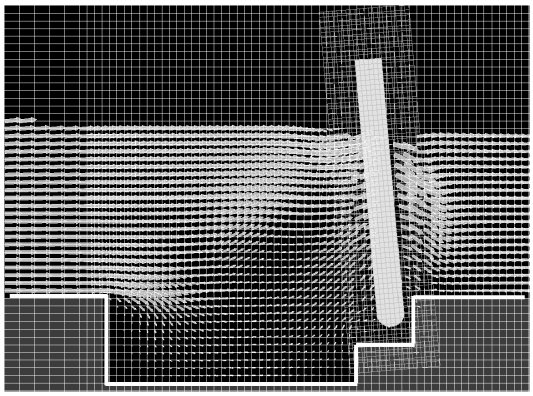

(c) Gate angle: 85 deg.

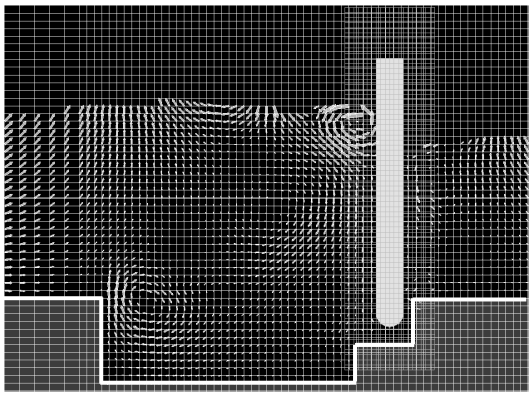

(f) 0.64 s after standing up

Figure 11. Snapshots of flow vectors in numerical simulation

Periodic wave experiments. Figure 12 shows an example of time series of numerical water elevations outside and inside and the flap-gate motions against periodic waves. The results at H31, H42 and H43 correspond to output points shown in Fig.8. As shown in Fig.12, the waves were transmitted to onshore side at H43 which located behind the flap-gate model. This is due to the flap-gate motions. The wave amplitude at H42 is changed after reflective waves from the flap-gate have arrived at H42.

Figure 13 shows the time series of flap-gate motions in the physical model experiments and the numerical simulations. The vertical axes show the flap-gate angle from the initial position normalized by the incident wave amplitude and the horizontal axes are the normalized time with the incident wave period, respectively. Figures 13 and 14 are different conditions of incident wave steepness and figures (a), (b) and (c) are results for different wave periods of 1.44 s, 1.81 s and 2.17 s, respectively. These wave periods correspond to 8 s 10 s and 12 s in the prototype scale, respectively. Moreover, the maximum and minimum angles of the flap-gate motions against periodic waves are shown in Fig.15.

As shown in Fig.13, Fig.14, and Fig.15, the maximums and the minimums of the numerical flap-gate motion are a little smaller than the experimental results. However, the numerical model gives satisfactory accurate predictions. The numerical flap-gate motion in case of H/L = 0.02 is smaller than the numerical one in the case of H/L = 0.04 since the grid size in this model is not enough to solve the flap-gate motions against small amplitude waves. The experimental result shows the flap-gate motions is increased and ranges of the flap-gate motions transfer upward as the incident wave period becomes longer. Numerical results agree with experimental results.

From the comparisons, it is confirmed that the developed numerical model is valid to predict flap-gate motions accurately. However, there are some minor differences between the experimental and numerical results. Numerical flow field is not affected by the side wall of wave channel and it is not considered in the two-dimensional numerical simulation. The momentum diffusion to the width direction was not generated and thus large scale vortexes tend to occur in the flow field relatively. These flows which affect the added mass of the numerical flap-gate cause differences between the experimental and numerical results. This part is required more careful validation and adequate turbulence model is required for modeling.

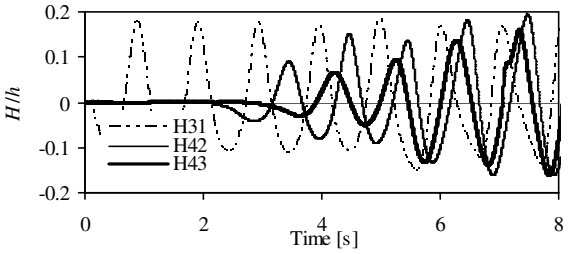

(a) Time series of water elevations at H31, H42 and H43

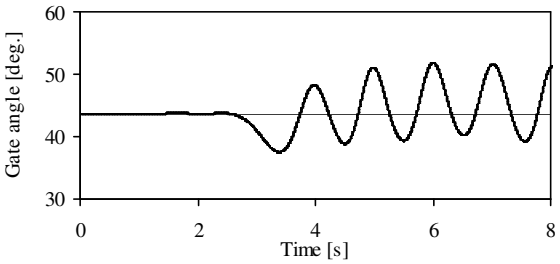

(b) Time series of the flap-gate motion

Figure 12. Example of simulation results of water elevations and flap-gate motion

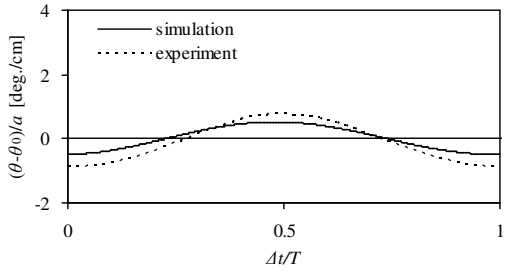

(a) T = 1.44 s

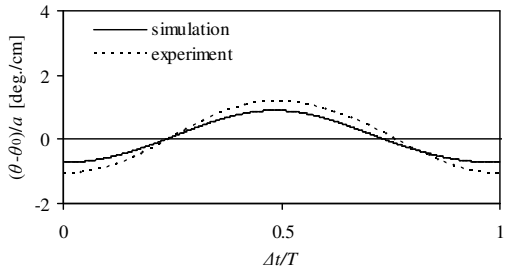

(b) T = 1.81 s

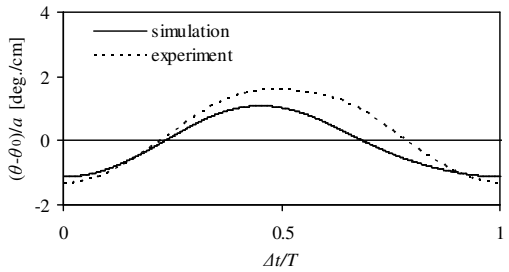

(c) T = 2.17 s

Figure 13. The flap-gate motion against a periodic wave; *H/L*=0.02

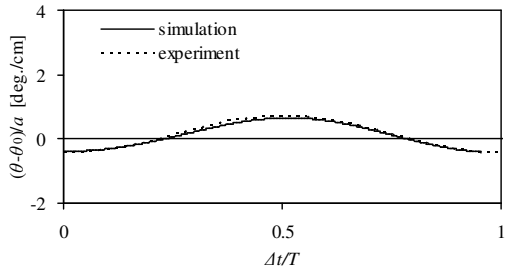

(a) T = 1.44 s

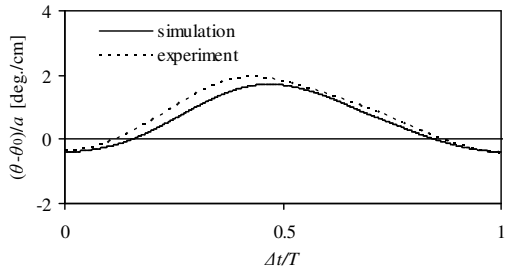

(b) T = 1.81 s

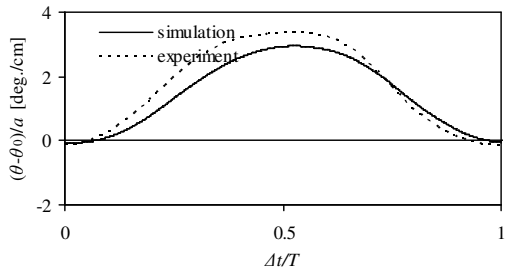

(c) T = 2.17 s

Figure 14. The flap-gate motion against a periodic wave; *H/L*=0.04

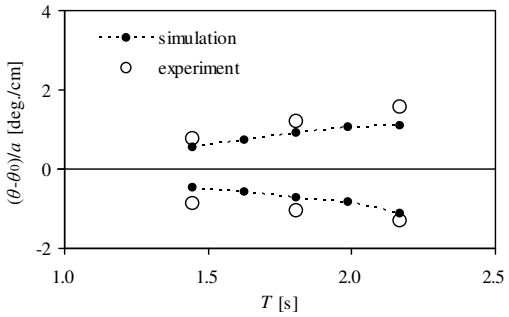

(a) H/L=0.02

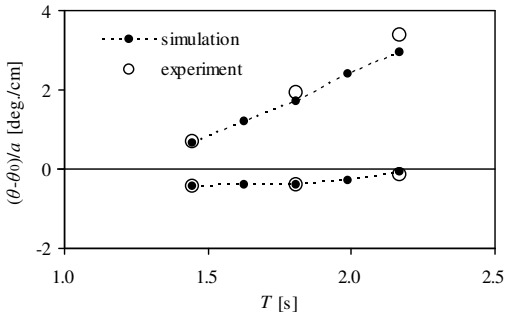

(b) H/L=0.04

Figure 15. Maximum and minimum of the flap-gate motions

CONCLUSIONS

The numerical model combining the overset grid method and the level set method was developed to simulate flat-gate motion under wavy environment. The flap-gate responses to solitary and periodic waves were estimated by this model and were evaluated by the hydraulic experiments. The main results are as follows:

- The propagation of solitary waves and periodic waves and the surface elevations related with the flap-gate motions were well simulated by the numerical model.
- The numerical accuracy of flap-gate motions due the solitary wave can be verified by the experimental results.
- The characteristics of numerical flap-gate motions against the periodic waves were well corresponded to the experimental results.

ACKNOWLEDGMENT

A part of this study was supported by a Grant-in-Aid for Scientific Research (KAKENHI) (#20360220).

REFERENCES

Lewin, J., and Scotti, A. (1990). The flood-prevention scheme of venice: experimental module, *Water and Environment Journal*, pp.70-77.

Kimura, Y., Niizato, H., Nakayasu, K., Yasuda, T. and Mase, H. (2009). Experimental study on mooring characteristics of flap type gate against tsunami and storm surge lying down on a seabed, *Annual Journal of Civil Engineering in the Ocean*, *JSCE*, Vol.25, pp.93-98 (in Japanese).

Kimura, Y., Niizato, H., Nakayasu, K., Yasuda, T. and Mase, H. (2009). Experimental study on response characteristics of flap gate breakwater against waves, *Annual Journal of Coastal Engineering*, *JSCE*, Vol.56, pp.806-810 (in Japanese).

Kimura, Y., Niizato, H., Nakayasu, K., Yasuda, T. and Mase, H. (2010). Hydraulic model experiments on response of flapgate breakwater to wave and tsunami, *Annuals of DPRI*, *Kyoto Univ*., Vol.53, B-2 (in Japanese), in press.

Kiyomiya, O., Shimosako, K., Yui, T., Yamashita, S., Shiina, M. and Tsuchiya, M. (2006). Analysis for rising and sinking motion of a flap-type gate in a still water, *Annual Journal of Civil Engineering in the Ocean*, *JSCE*, Vol.22, pp.691-696 (in Japanese).

Matsuno, K., Yamakawa, M. and Satofuka, N. (1998). Overset adaptive-grid method with applications to compressible flows, *27th Computers & Fluids,* pp.599-610.

Obata, M., Nakao, T., Satofuka, N. and Morinishi, K. (1993). Numerical solution of 2-dimentional flows through butterfly valve using overset grid technique, *Technical Journal, JSME*, Vol.59, pp.220-226 (in Japanese).

Shirai, S., Fujita, T., Kimura, Y., Yamaguchi, E. and Nakayasu, K. (2006). Experimental study of the flap type gate as a tsunami countermeasure, *Annual Journal of Civil Engineering in the Ocean*, *JSCE*, Vol.22, pp.577-582 (in Japanese).

Tanno, I., Morinishi, K., Matsuno, K. and Nishida, H. (2004). Simulation around arbitrary shape body with virtual flux method on Cartesian grid, *Technical Journal*, *JSME*, Vol.70, pp.9-16 (in Japanese).

Tomita, T., Kawasaki, K., and Shimosako, K. (2003). Wave forces acting on flap-type storm surge barrier and waves transmitted on it, *Proc. of 13th Int. Offshore and polar Eng. Conf*., pp.639-646.

Wada, Y., Morinishi, K. and Matsuno, K. (2005). Numerical simulation of bubble coalescence and separation by level set method, *Computing Fluid Dynamics 2008*, *JSFM*, pp.1-6 (in Japanese).

Yang, C., and Mao, Z. (2005). Numerical simulation of interphase mass transfer with the level set approach, *60th Chemical Eng. Science*, pp.2643-2660.